

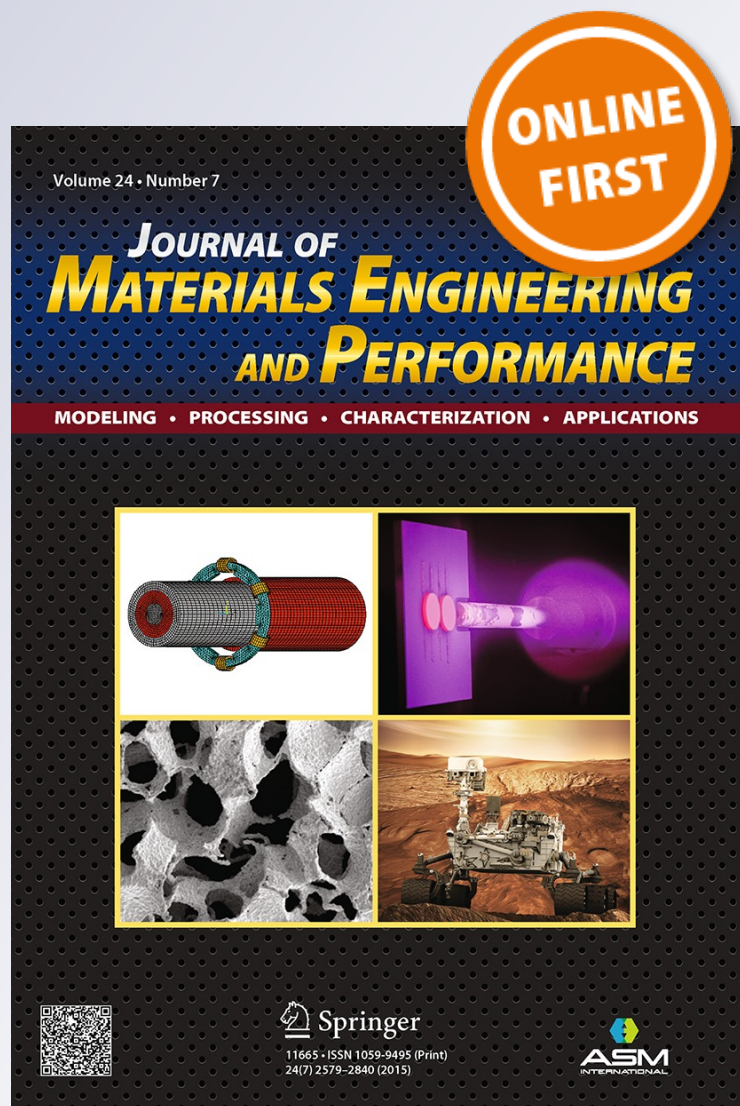
# *Investigation of Porosity Changes in Cast Ti6Al4V Rods After Hot Isostatic Pressing*

**Anton du Plessis & Pierre Rossouw**

**Journal of Materials Engineering and Performance**

ISSN 1059-9495

J. of Materi Eng and Perform  
DOI 10.1007/s11665-015-1580-4



**Your article is protected by copyright and all rights are held exclusively by ASM International. This e-offprint is for personal use only and shall not be self-archived in electronic repositories. If you wish to self-archive your article, please use the accepted manuscript version for posting on your own website. You may further deposit the accepted manuscript version in any repository, provided it is only made publicly available 12 months after official publication or later and provided acknowledgement is given to the original source of publication and a link is inserted to the published article on Springer's website. The link must be accompanied by the following text: "The final publication is available at [link.springer.com](http://link.springer.com)".**

# Investigation of Porosity Changes in Cast Ti6Al4V Rods After Hot Isostatic Pressing

Anton du Plessis and Pierre Rossouw

(Submitted March 28, 2015; in revised form May 27, 2015)

The porosities of cast Ti6Al4V rods were investigated nondestructively using x-ray microcomputed tomography (microCT) before and after HIP. This allowed the visualization and quantification of porosity changes in the same samples, which indicate excellent pore closure for large pores. This is the first reported application of x-ray microCT for direct analysis of investment casting porosity before and after HIP. The method shows promise for further investigations using delayed HIP treatments or monitoring of pore closure at further varying HIP cycle settings. The nondestructive nature of the analysis has resulted in the interesting observation of small subsurface pores ( $<250\ \mu\text{m}$ ) unaffected by hot isostatic pressing in two of the samples.

**Keywords** casting, hot-pressing, porosity, x-ray tomography

## 1. Introduction

Hot isostatic pressing (HIPping) is a well-known method to reduce porosity in castings and improve material properties (Ref 1). A metal object is heated and put under pressure by inert gas, effectively causing internal pores to close while any open pores connected to the surface will remain. HIP treatment has been applied to titanium castings since the 1980s with great success (Ref 2). In fact, the first image of pores before and after HIPping are shown in (Ref 2), though not from the same sample in that case. Defects in titanium investment castings are reasonably well understood, also in relation to HIP treatment (Ref 3). The process of pore annihilation during HIPping has been studied in detail by interrupted HIP tests and metallography and electron microscopy (Ref 4).

MicroCT is a well-known material characterization and measurement tool, especially useful for quantitative 3D measurements (Ref 5). A typical microCT analysis can be reasonably simple especially for porosity, as demonstrated in (Ref 6). X-ray microCT has been used for porosity analysis of various metals including titanium castings (Ref 7). Nicoletto et al (Ref 8, 9) have done direct comparisons of 2D metallography and 3D x-ray CT for pore analysis of cast aluminum alloys, indicating the correlation between the two methods and how 3D pore morphology can affect material stress and fatigue life. Recently, x-ray CT was used for pore

visualization and analysis of electron beam melted titanium parts (Ref 10).

Wan et al (Ref 11) have analyzed aluminum die-cast samples before fatigue tests and correlated the initiation sites of cracks after fatigue tests to their origin, showing that 80% initiated from pores and most of these from large gas pores, although the pore's location relative to the surface also played a role and some shrinkage pores also acted as initiation sites. In a different study also on aluminum die-cast samples, Kuwazuru et al (Ref 12) found that specifically shrinkage pores were related to initiation sites of cracks, although the samples seem to be of higher average porosity than those investigated by Wan et al (Ref 11).

Thus far, there have been no reports on the use of x-ray tomography for quantitative porosity analysis pre and post HIP treatment. In this work, the porosity changes induced by HIP treatment were investigated for a series of six titanium castings, using x-ray microCT before and after treatment. The sample dimensions (long rods) allowed a particularly high-resolution analysis using multiple scans. The full 3D nondestructive nature of the analysis provides quantitative information on individual pore size changes. In this case, the HIPping was very successful as expected for this type of casting process (for this size and type of porosity and sample size). The 3D nature of the analysis has provided an unexpected result in the finding of isolated small ( $<250\ \mu\text{m}$ ) pores very near but definitely under the surface of the sample.

## 2. Experimental Details

Titanium 64, Ti6Al4V, due to its low density of  $4.4\ \text{g cm}^{-3}$  and high melting temperature with a liquidus temperature of  $1663\ ^\circ\text{C}$ , is prone to shrinkage porosity. This is caused by the high cooling rate and short feeding distance as a result of the high temperature difference between the mold and the metal.

Mold temperatures have to be kept as low as possible to reduce the metal–mold reaction as titanium reduces most refractories causing absorption and diffusion of interstitial oxygen and refractory metals such as zirconium. Oxygen is responsible for the formation of the very hard and brittle alpha

Electronic supplementary materialThe online version of this article (doi:10.1007/s11665-015-1580-4) contains supplementary material, which is available to the authorized users.

**Anton du Plessis**, CT Scanner Facility, Central Analytical Facilities, Stellenbosch University, Stellenbosch, South Africa and Physics Department, Stellenbosch University, Stellenbosch, South Africa; and **Pierre Rossouw**, CSIR Materials Science and Manufacturing, Pretoria, South Africa. Contact e-mail: anton2@sun.ac.za.

case on the surface of the casting but due to diffusion causes a hardness gradient from the surface into the casting which can be measured using micro-hardness techniques but is not visible in the microstructure.

$\text{Ø}15 \times 210 \text{ mm}^2$ -long rod samples were produced using investment casting with Ti6Al4V wrought bar from a single mastermelt. The molds were produced at the CSIR using an Ytria-based and Ytria-stabilized Zirconia face coat system. Molds were cast using copper skull melting under vacuum at the University of Hannover as no facility is currently available in South Africa. Molds were cooled under vacuum for 2 min before removal from the vacuum furnace. The molds were then removed from the insulated tin immediately after removal from the furnace and cooled in still air. The casting process is given in Fig. 1. Figure 2 shows castings after removal of molds, with those that were produced using the Ytria-based face coat castings at the top.

Six of the eight rods per mold, randomly selected, were sent to Bodycote in Belgium for the standard HIP process used for titanium

castings,  $920 \pm 10 \text{ °C} @ 100 \pm 5 \text{ MPa}$  for  $120 \pm 30 \text{ min}$ . Chemical and gas analysis were performed, and mechanical samples were produced and tensile properties determined in relation to ASTM 8E. This process was used to qualify the casting process, resulting in all molds passing the mechanical tests, except one. Mechanical tests were performed on one rod per mold, according to the AMS4926A Standard Investment cast and hot isostatically pressed Ti6Al4V section 3.6 minimum requirement.

Remaining untreated rods were then randomly selected and supplied to Stellenbosch University for microCT scanning before being submitted to Avure in Sweden for HIP processing using different parameters listed in Table 1. Cycle number refers to chronological order of HIP processing, not increasing numbers of cycles. A total of six rods were selected for microCT analysis, from cycles 1, 3, 4, 5, 6, covering both high and low cooling rates as well as different HIP temperature and pressure conditions. Samples from cycle 2 were scanned before HIP but were late to return from Avure due to problems and were therefore not selected for post-HIP scans.



Fig. 1 The melting and casting process

A commercial x-ray microCT scanner was used in this study, the General Electric Phoenix V|Tome|X L240, housed at the Stellenbosch CT Scanner Facility. X-ray scan settings were 200 kV, 100  $\mu$ A, with 1200 images acquired in one full rotation of the sample. Copper filters of 1.8 mm were used to reduce beam hardening artifacts. Scan resolution was set to 30  $\mu$ m, with multi-scan option enabled resulting in up to seven scans required to image the entire sample at 30  $\mu$ m. This involves an automatic stitching of volumes using the system software, which is visible in grayscale contrast at the stitched positions in slice images (from side views). Additional scans at 118  $\mu$ m of the entire sample were performed at once (called fast scans), which could be used for reference and for easy access, since the volume sizes are small. One additional high-resolution scan of sample S10E was done, in the location of the largest pore present before HIP treatment, with the high-resolution scan done after HIP treatment. Sample S10E was also cut into smaller disks and scanned at further higher resolution settings. Reconstruction was done with the system-supplied Datos reconstruction software.

Analysis was performed with Volume Graphics VGStudio Max 2.2. The analysis procedure was identical in each case and made use of automated tools in VGStudioMax to ensure no biasing of results; the method is described below. Two volumes are loaded (before and after scans) and analysis is performed identically on both. The sample is selected by region growing

air and inverting the data. An automatic surface fit using the advanced function is applied to the extracted rod, a region of interest is selected based on this surface, this is inverted and a closing function of 1 voxel is applied. This is used as mask for a defect analysis using custom defect mask option, filtering the data to find pores of a minimum volume of 16 voxels up to a maximum diameter of 100 mm.

### 3. Results and Discussion

A defect analysis of each pair of before–after volumes was performed identically as discussed in the previous section. The side-by-side views of the before and after volumes are shown in 3D with color coding of pores based on their volume, in Fig. 3, 4, and 5. Figure 3 is a 3D representation with the material semi-transparent to highlight the location of pores. 3D videos of all six samples are available as supplementary material. Figure 4 is a top-view 2D slice image, showing the absence of any void in the location of the largest void before HIPping. Figure 5 shows a side view indicating the same result across all pores in the center of the rod. The top view shows some circular ring artifacts, while the side view shows some stitching artifacts due to multiple scans taken to ensure highest resolution.

Average porosity values shown in Table 2 are calculated from the automated defect analysis: values are taken from actual volumes of selected pores found and added together. All



Fig. 2 Sample rods after casting with mold removed

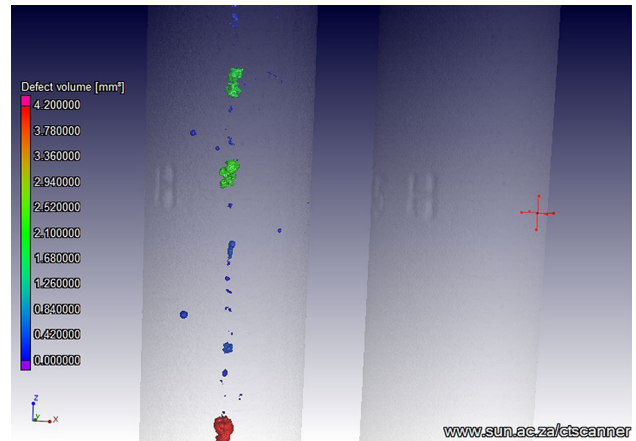
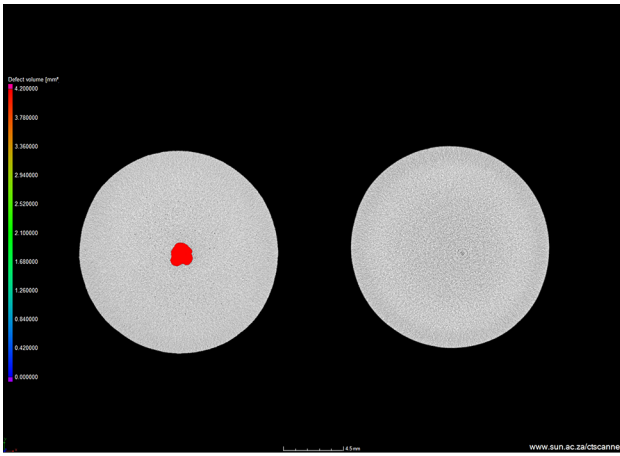


Fig. 3 3D semi-transparent view of one region of the rod S5H before (left) and after (right) HIP treatment. The cross indicates the location of one small pore identified post HIP treatment. 3D videos available as supplementary material

Table 1 Different HIP parameters

Cycle #	Pressure, MPa	Temperature, °C	Hold time, h	Cooling type	Cooling rate between 950-400 °C, °C/min	Rod nr
1	170	1050	1.5	URQ	1070	S5H,S10E
2	170	950	2	URQ	1640	S1F,S4A
3	100	1050	2	URC	180	S6A
4	100	980	2	URC	193	S8F
5	100	980	4	URC	191	S7A
6	170	930	2	URC	194	S13G

(URQ ultra rapid quench), (URC ultra rapid cool)



**Fig. 4** Top slice view of sample S5H before (left) and after (right) HIP treatment. The pore diameter is 2.7 mm before HIP

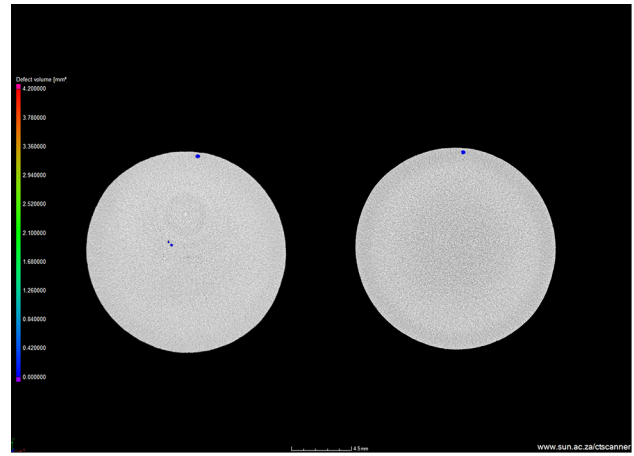


**Fig. 6** Slice images before and after HIPping highlighting one subsurface pore which remains

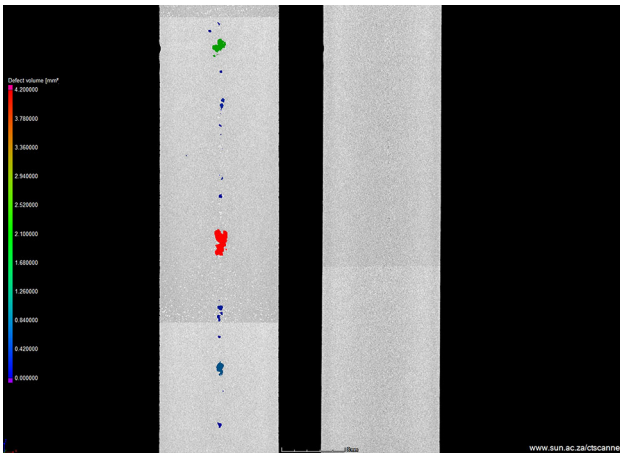


**Fig. 5** Side view of sample S5H before (left) and after (right) HIPping

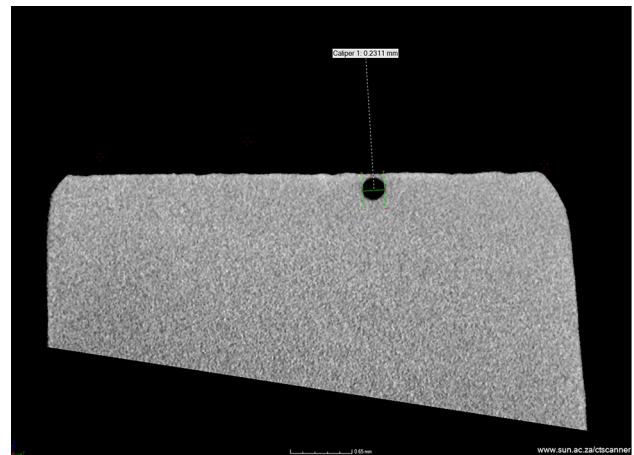


**Fig. 7** Subsurface pore post HIP

**Table 2 Total volumetric (average) porosity results**

Sample name	Before HIP %	After HIP %
S10E	0.077	0.0003
S5H	0.073	0.00006
S13G	0.092	0
S7A	0.059	0
S6A	0.079	0
S8F	0.074	0

these values are relevant for detected pores in the size range 0.06–100- $\mu\text{m}$  diameter, ie., pores smaller than 60  $\mu\text{m}$  would not be detected clearly enough to quantify.

The two samples containing some small pores after HIPping are from cycle 1, as given in Table 1, which has the shortest hold time and the fastest cooling rate of those analyzed by CT scans post HIP.

A close-up scan (field of view, 15 mm) of the region in sample S10E at the location of the largest pore (before HIP treatment) was done after HIP treatment, to see if any smaller pore remains or if density variations could be detected at the exact position of the largest pore before HIP (through greyscale

variations). A scan at 10- $\mu\text{m}$  resolution could not resolve any features at all at this location and indicates that no pores are present in the vicinity of the large pore before HIPping, down to 20- $\mu\text{m}$  diameter, and no low-density regions are detected.

Some unexpected isolated pores near the surfaces of samples S10E and S5H were identified even though the interiors of these samples are fully dense. A good indicative slice image is shown in Figure 6 (sample S10E), where the internal pore has closed but two isolated subsurface pores remain. Three disk-shaped sections were cut from the rod at the locations of these subsurface pores, for higher resolution scans. One such scan at a higher resolution of 5.6  $\mu\text{m}$  is shown in Figure 7, clearly showing in this slice image that the pore is below the surface. Figure 8 is a 3D view of the same region at high resolution indicating four such pores all are just under the surface, all very spherical in shape. These pores have diameters of 259, 203, 115, and 91  $\mu\text{m}$ , and their nearest edges were measured as 41, 55, 30, and 64  $\mu\text{m}$  from the surface of the rod, respectively.

The presence of these subsurface pores can possibly be explained by the hard and brittle alpha case layer, which may contain small micro- or nanoscale cracks or interconnected pore networks below the resolution limit of the CT scan. If some of these cracks or nanopores connected the large pore to the

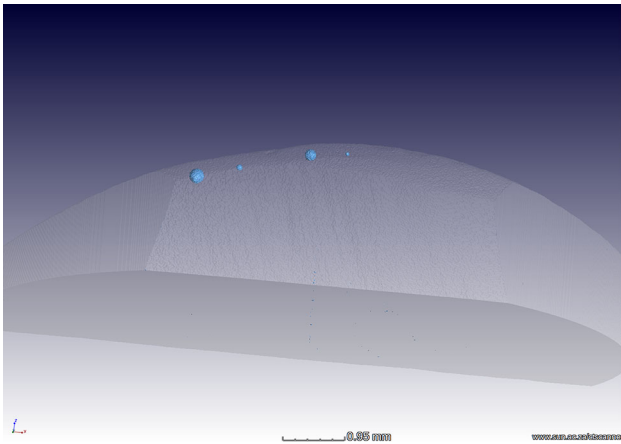


**Fig. 8** 3D view of subsurface pores from 5.8- $\mu\text{m}$  scan (4 pores in blue). 3D video available as supplementary material

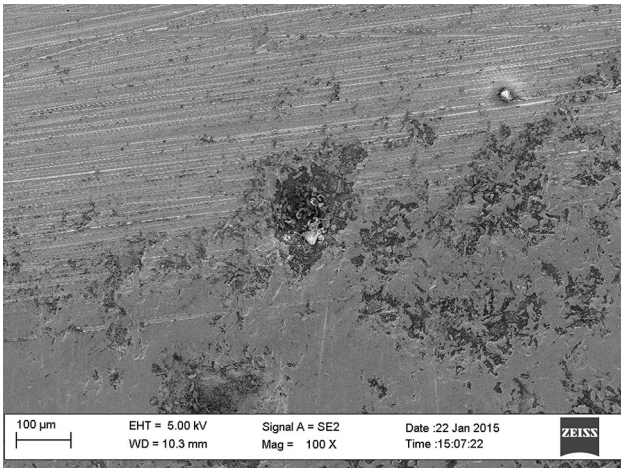


**Fig. 9** SEM image of subsurface pore, taken after polishing off a thin layer of surface material

exterior, HIP treatment would not be effective, explaining its presence.

A further investigation was done by locating the expected position of the largest subsurface pore in the scanned disk-shaped sample shown in Fig. 7 and 8, and polishing it down very slightly followed by SEM imaging. Figure 9 shows the pore as it has been exposed by the polishing. Though not conclusive, the image shows surface roughness which could be associated with microcracks or pores.

## 4. Conclusion

A series of 6 Ti4Al6V cast rods were subjected to x-ray microCT scans before and after HIPping. The results indicate

excellent pore closure, even for the largest pores. The six rods had average porosities in the range of 0.06–0.08% before HIPping, with only two having any detectable pores after HIPping, leaving them at 0.0003 and 0.0006%. The largest pore diameters before and after HIPping for sample S10E were 2.7 and 0.2 mm respectively, while the largest pore entirely closed and the remaining small pores are near the surface of the part.

Some small isolated pores were identified just under the surface of two samples. It is speculated that the alpha case outer layer results in connectivity between the pore and the surface through microcracks or nanoscale pore networks resulting in them being unaffected by HIPping. This is correlated with both samples coming from the same HIP cycle with the fastest cooling rate.

## Acknowledgments

The South African Department of Science and Technology and the CSIR have funded aspects of this work and are gratefully acknowledged.

## References

1. H.V. Atkinson and S. Davies, Fundamental Aspects of Hot Isostatic Pressing: An Overview, *Metall. Mater. Trans. A*, 2000, **31A**
2. R.L. Saha and K.T. Jacob, Casting of Titanium and Its Alloys, *Def. Sci. J.*, 1986, **36**, p 2
3. J.D. Cotton, L.P. Clark, and H.R. Phelps, Titanium Investment Casting Defects, *JOM*, 2006, **58**(6), p 13–16
4. A. Epishin, B. Fedelich, T. Link, T. Feldmann, and I.L. Svetlov, Pore Annihilation in a Single-Crystal Nickel-Base Superalloy During Hot Isostatic Pressing: Experiment and Modelling, *Mater. Sci. Eng. A*, 2013, **586**, p 342–349
5. E. Maire and P.J. Withers, Quantitative X-ray Tomography, *Int. Mater. Rev.*, 2014, **59**(1), p 1–43
6. A. du Plessis and P. Rossouw, X-ray Computed Tomography of a Titanium Aerospace Investment Casting. *Case Stud. Nondestruct. Test. Evaluat.*, 2015, **3**, p 21–26
7. A. du Plessis, B.J. Olawuyi, W.P. Boshoff, and S.G. le Roux, Simple and Fast Porosity Analysis of Concrete using X-ray Computed Tomography. *Mater. Struct.*, 2014. doi:10.1617/s11527-014-0519-9
8. G. Nicoletto, G. Anzelotti, and R. Konecná, X-ray Computed Tomography vs. Metallography for Pore Sizing and Fatigue of Cast Al-Alloys, *Procedia Eng.*, 2010, **2**, p 547–554
9. G. Nicoletto, R. Konecná, and S. Fintova, Characterization of Microshrinkage Casting Defects of Al-Si Alloys by X-ray Computed Tomography and Metallography, *Int. J. Fatigue*, 2012, **41**, p 39–46
10. S. Tammis-Williams, H. Zhao, F. Léonard, F. Derguti, I. Todd, and P.B. Prangnell, XCT Analysis of the Influence of Melt Strategies on Defect Population in Ti-6Al-4V Components Manufactured by Selective Electron Beam Melting, *Mater. Charact.*, 2015, **102**, p 47–61
11. Q. Wan, H. Zhao, and C. Zou, Effect of Micro-porosities on Fatigue Behavior in Aluminum Die Castings by 3D X-ray Tomography Inspection, *ISIJ Int.*, 2014, **54**(3), p 511–515
12. O. Kuwazuru, Y. Murata, Y. Hangai, T. Utsunomiya, S. Kitahara, and N. Yoshikawa, X-ray CT Inspection for Porosities and Its Effect on Fatigue of Die Cast Aluminium Alloy, *J. Solid Mech. Mater. Eng.*, 2008, **2**(9), p 1220–1231